

1 Abstract

Blind-thrust faults and well-mapped faults such as San Andreas, form a major risk for earthquakes in Southern California. Studies done by Shaw et al. (1996) & Weldon et al. (2005) point to the high hazard associated with the San Andreas fault, especially for tall buildings which are more sensitive to long period motions. Considered to be the most ductile of structural systems, in recent earthquakes, significant number of moment frame buildings had fracture in beam-to-column connections. Motivated by the large number of existing buildings of this type in the Los Angeles basin & the hazard posed by the San Andreas fault, we are conducting a suite of simulations to quantify the risk to these buildings from San Andreas earthquakes over the next 30 years. The procedure outlined by Krishnan et al. (2006) is being followed.

- Large number of stochastic source models are being generated for earthquakes in the magnitude range of 6.0 - 8.0. Unilateral rupture propagation (with rupture directivity from North - South & South - North) considered.
- Using SPEC3D, synthetic seismograms are generated at various sites across SoCal.
- FRAME3D models of two steel moment frame buildings in the 20-story class and one steel building in the 40-story class (dual lateral force-resisting system of braced frame core with perimeter moment frame) will be analyzed under the synthetic 3-component waveforms.
- Probabilistic economic losses will be computed at each location under each scenario. Finally, annualized losses will be computed by assigning probabilities of occurrence of each scenario over the next 30 years using the Uniform California Earthquake Rupture Forecast (UCERF 3.0).

2 Stochastic Slip Modeling

a. Slip generation for magnitude (M_w) 6.0-7.0 earthquakes

- Given M_w to be simulated, rupture area(A) is determined by Hanks & Bakun relation.
- Rupture length L is determined assuming seismogenic depth d to be 20km (constraint: minimum aspect ratio - length to depth of 1.0 is maintained)
- Fault area is discretized in $0.5 \text{ km} \times 0.5 \text{ km}$ patches to capture 2 sec. wave period.
- Log-normal distribution used to characterize slip. Mean and standard deviation are calculated using seismic moment vs. mean displacement relation and past earthquake data.
- Asperity studies by Somerville et al.(1999) are incorporated.

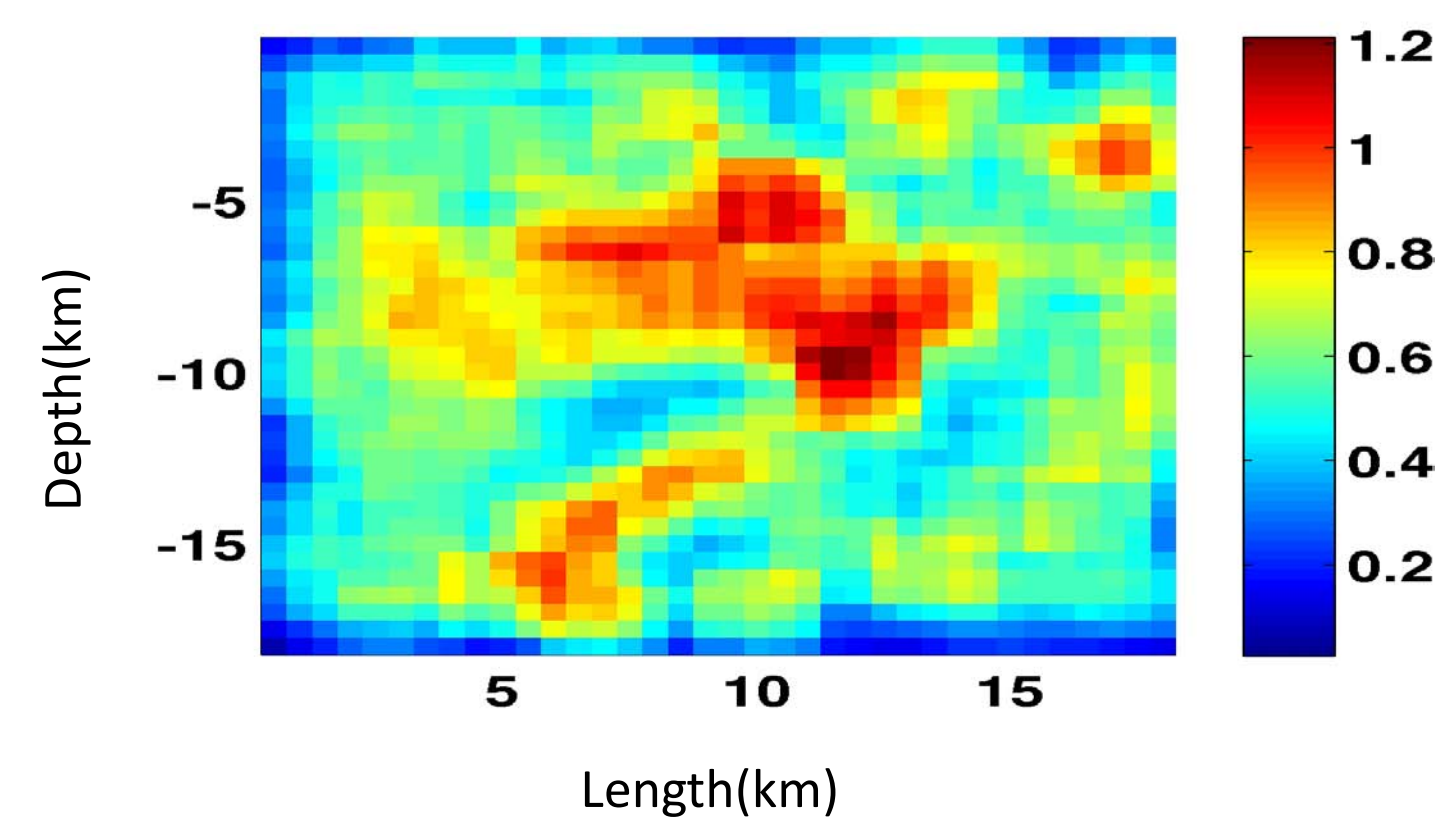


Fig.1: Single realization of slip on fault for M_w 6.5 earthquake

b. Slip generation for magnitude (M_w) 7.0-8.0 earthquakes

- Fault is segmented stochastically. The slip generation methodology for M_w 6.0-7.0 earthquakes is used to generate slip in each segment.
- Normal distribution (mean and standard deviation from studies by Klinger 2009) is used to determine segment length L_s , which is constrained to stay within one standard deviation of the mean.
- Segment mean slip is constrained to be greater than 10% of the standard deviation of all segment mean slips (to avoid negligible segment mean slip).

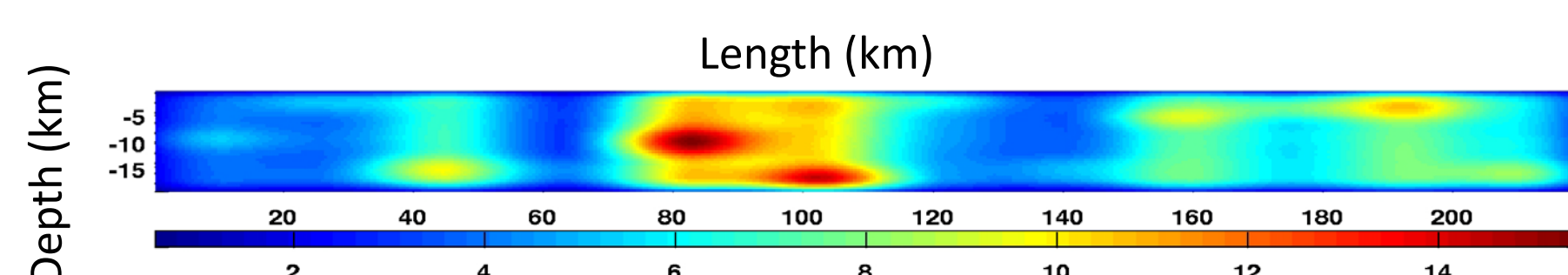


Fig.2: Single realization of slip on Fault for M_w 7.9 earthquake

3 Rupture Velocity

Whether rupture propagates at sub-Rayleigh or super-shear speeds depends upon the initial stress distribution on the fault.

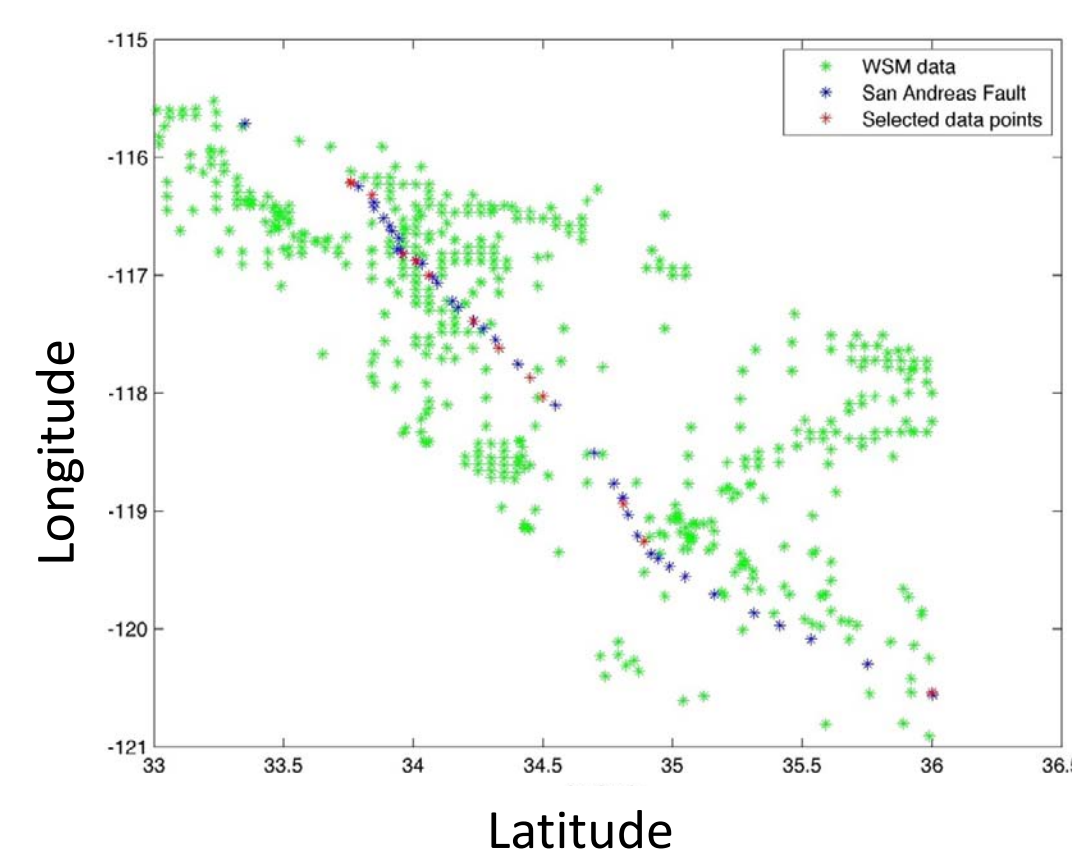


Fig.3: Location of data points available from World Stress Map (WSM) with principal stress orientation values & selected data points for San Andreas fault to determine stress distribution

Here the stresses on the fault are inferred from World stress maps. Two propagation scenarios are considered.

- Rupture ramps up to sub-Rayleigh speed of $0.87C_s$ and propagates at that speed for the remaining rupture length.
- Rupture ramps up to sub-Rayleigh speed and then transitions to the super-shear speed of $1.67C_s$ for the remaining rupture length.

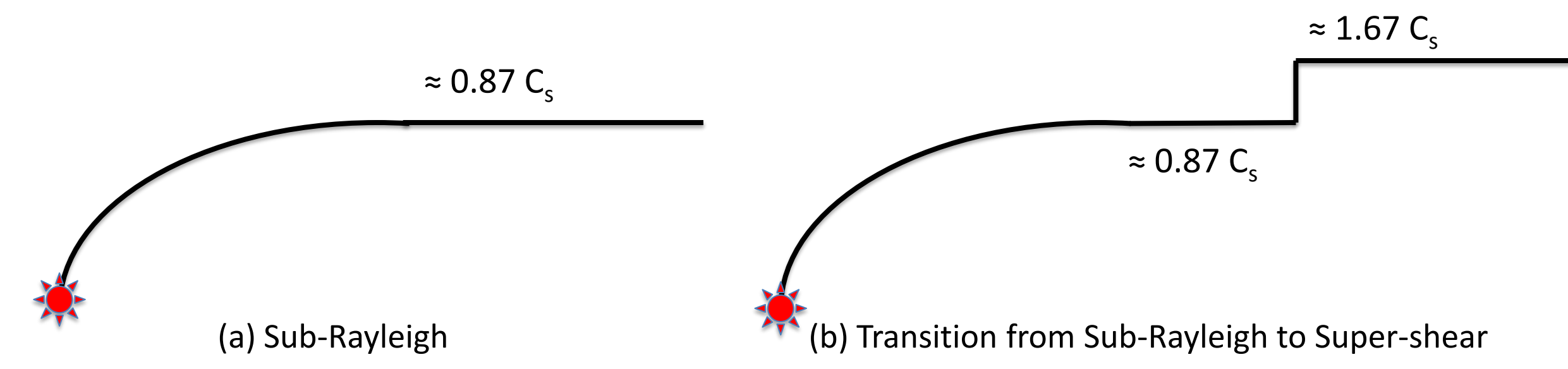


Fig.4: Rupture propagation scenarios being used in study based on initial stress distribution. A combination of critical transition length L_c & loading factor s is used to determine the scenario. Red star represents the hypocenter.

4 Source-Time Functions

Traditionally kinematic source-inversions represented source-time functions using triangular or modified sinusoidal curves. Given that these are empirical, we have chose to use source-time functions measured in laboratory earthquakes. However such data are limited to narrow ranges of sub-Rayleigh & super-shear speeds.

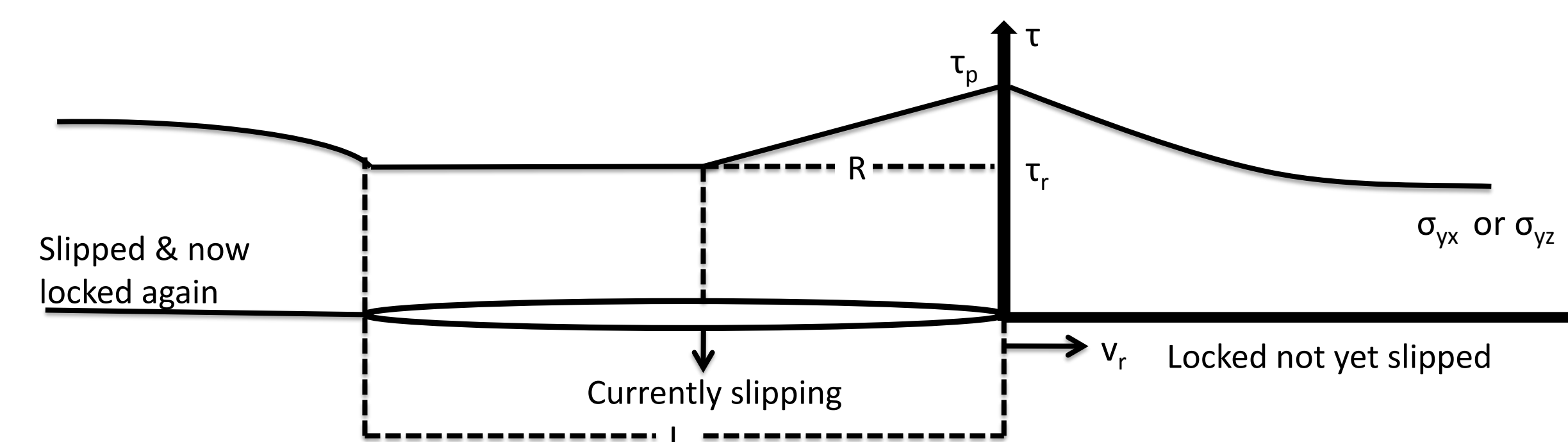


Fig.5: Non-Singular slip-pulse model used to determine source-time function in rupture-initiation zone.

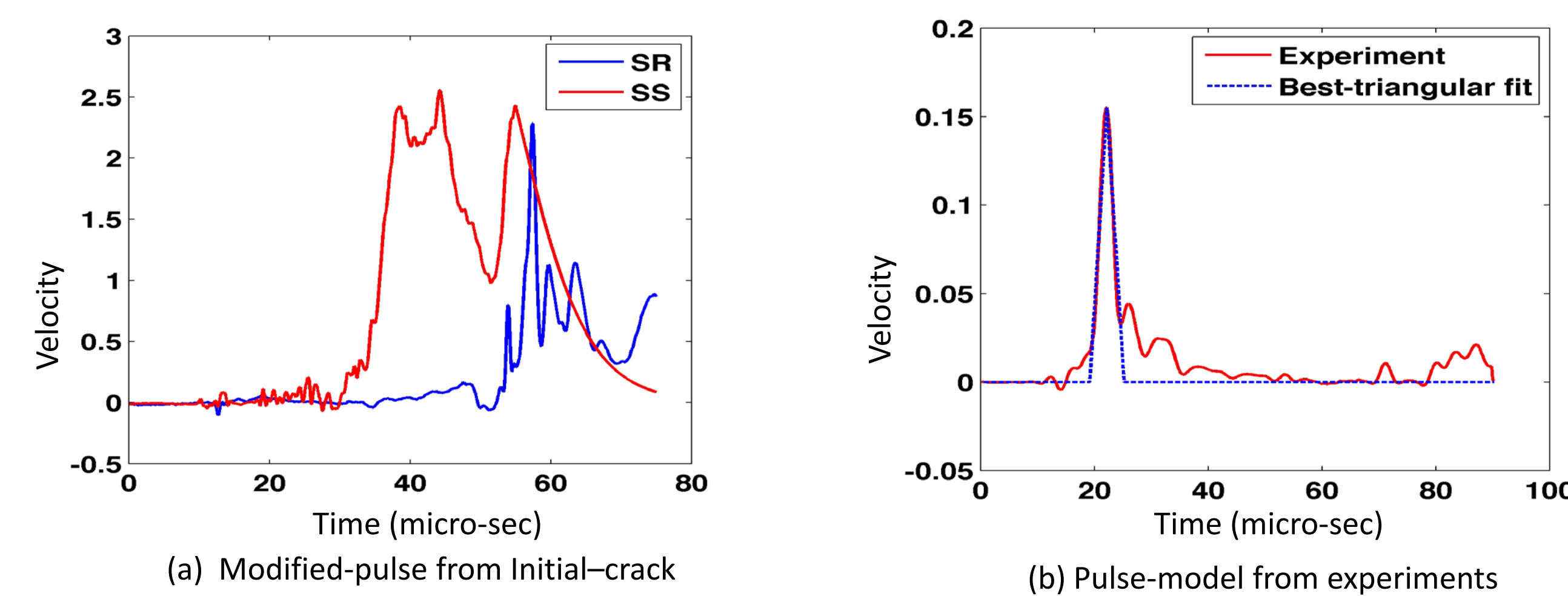
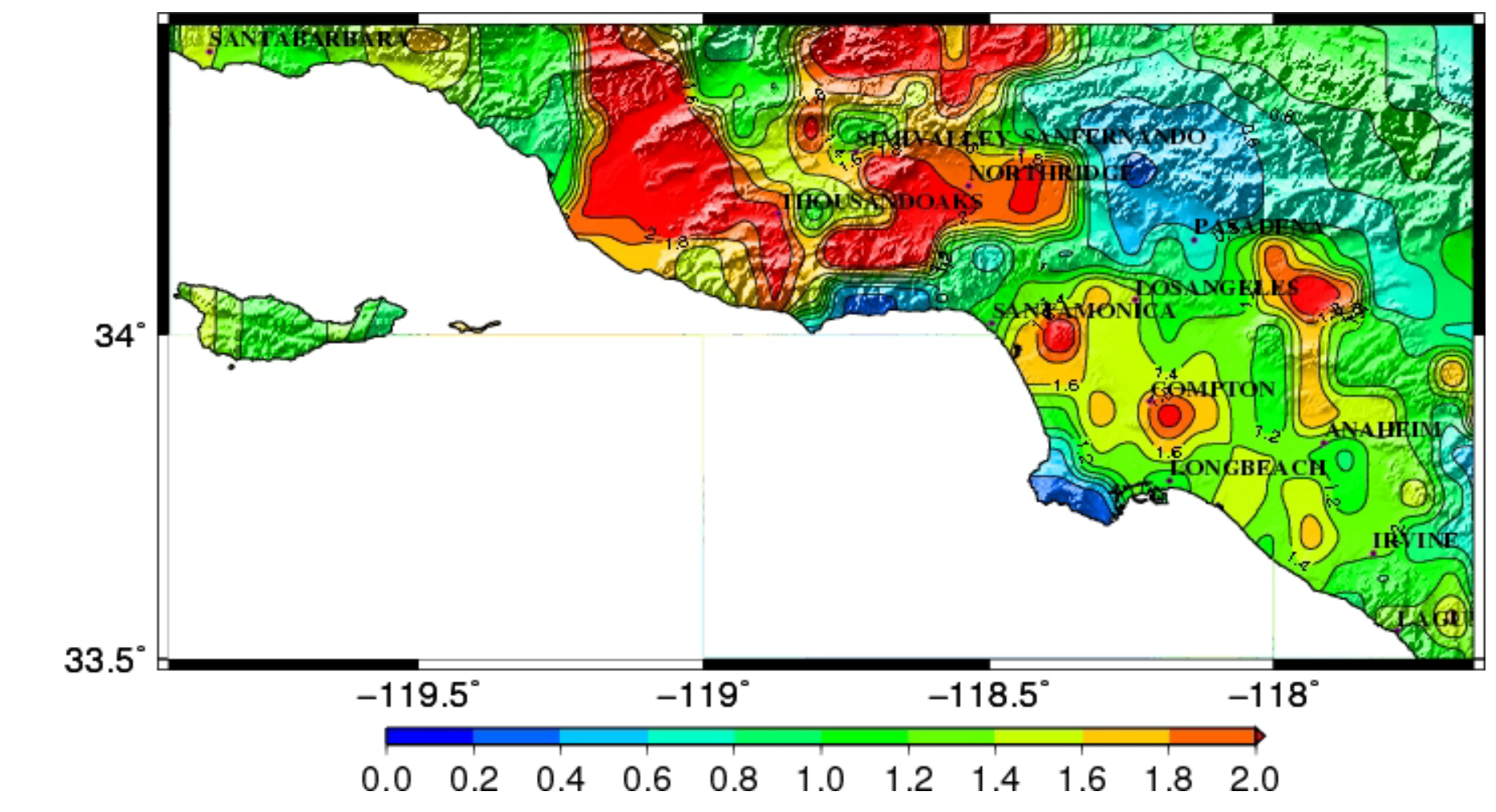
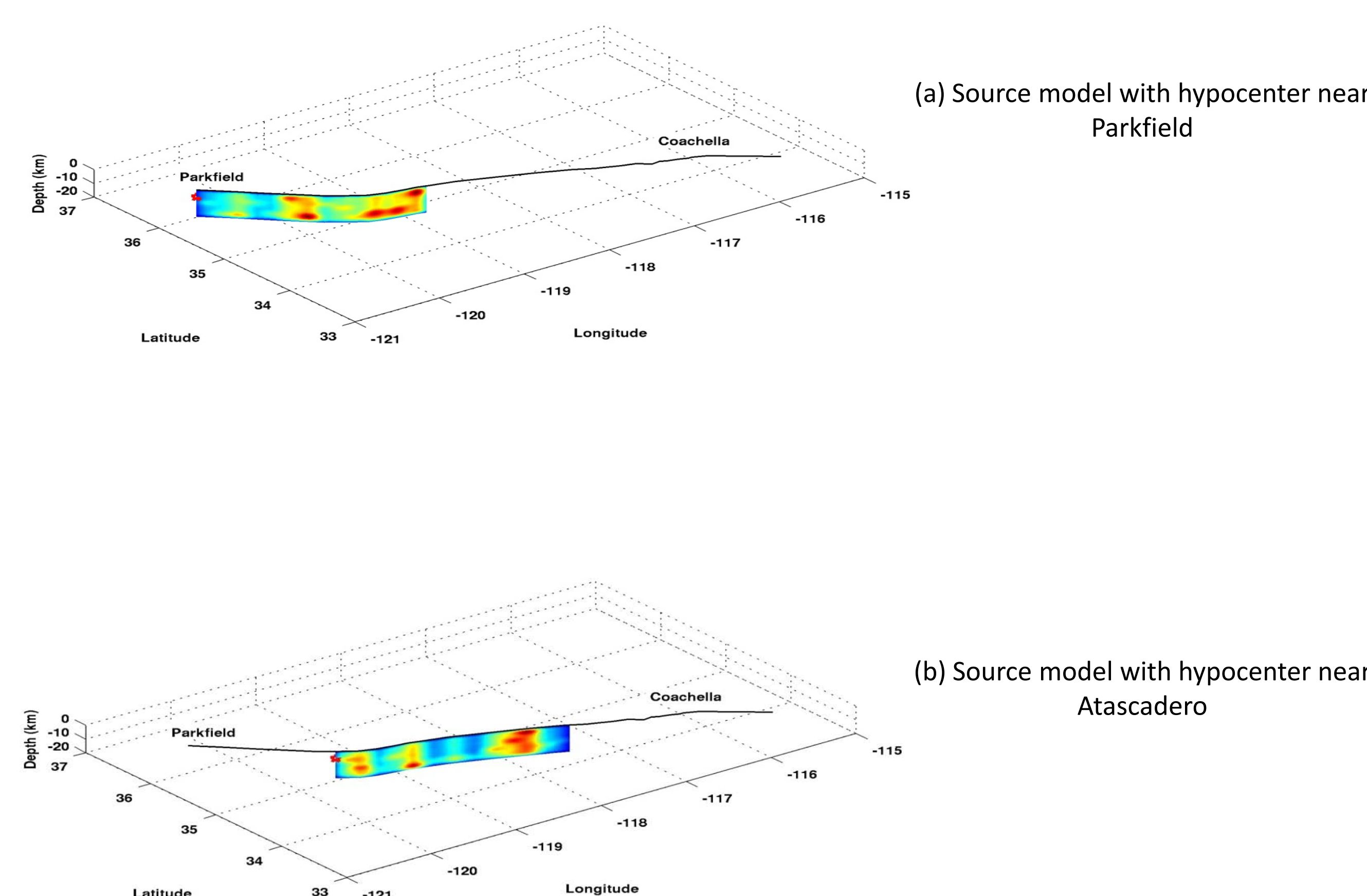


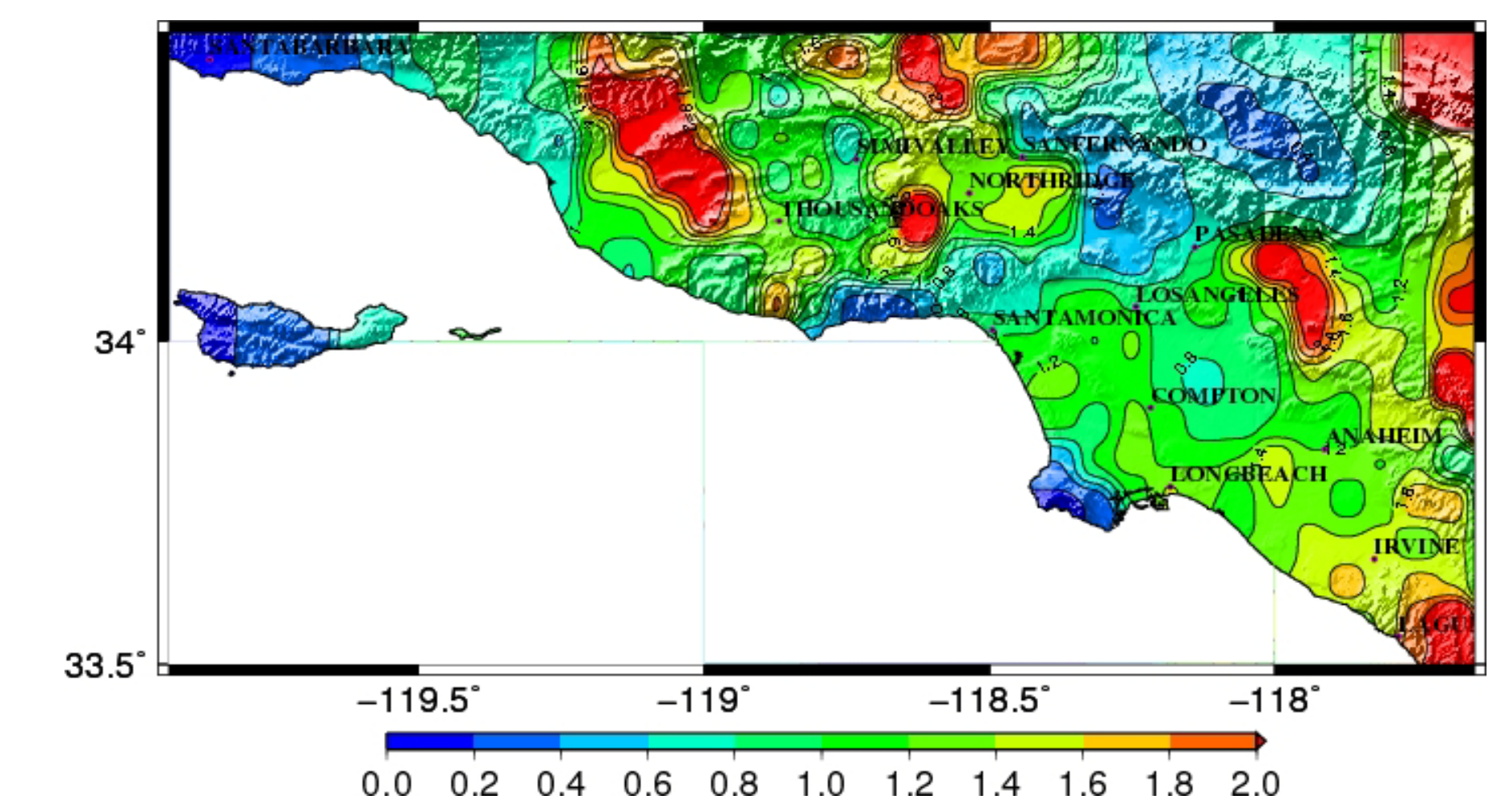
Fig.6: Source-time function measured in experiments in super-shear & sub-Rayleigh regimes. Scaling from experiments to real time is done by direct comparison of seismograms (experimental & real time) for trailing Rayleigh wave in the PS10 record from the Denali earthquake. Idealized representations of these functions would be incorporated to generate ground motions using SPEC3D

5 Ground Motion Simulations

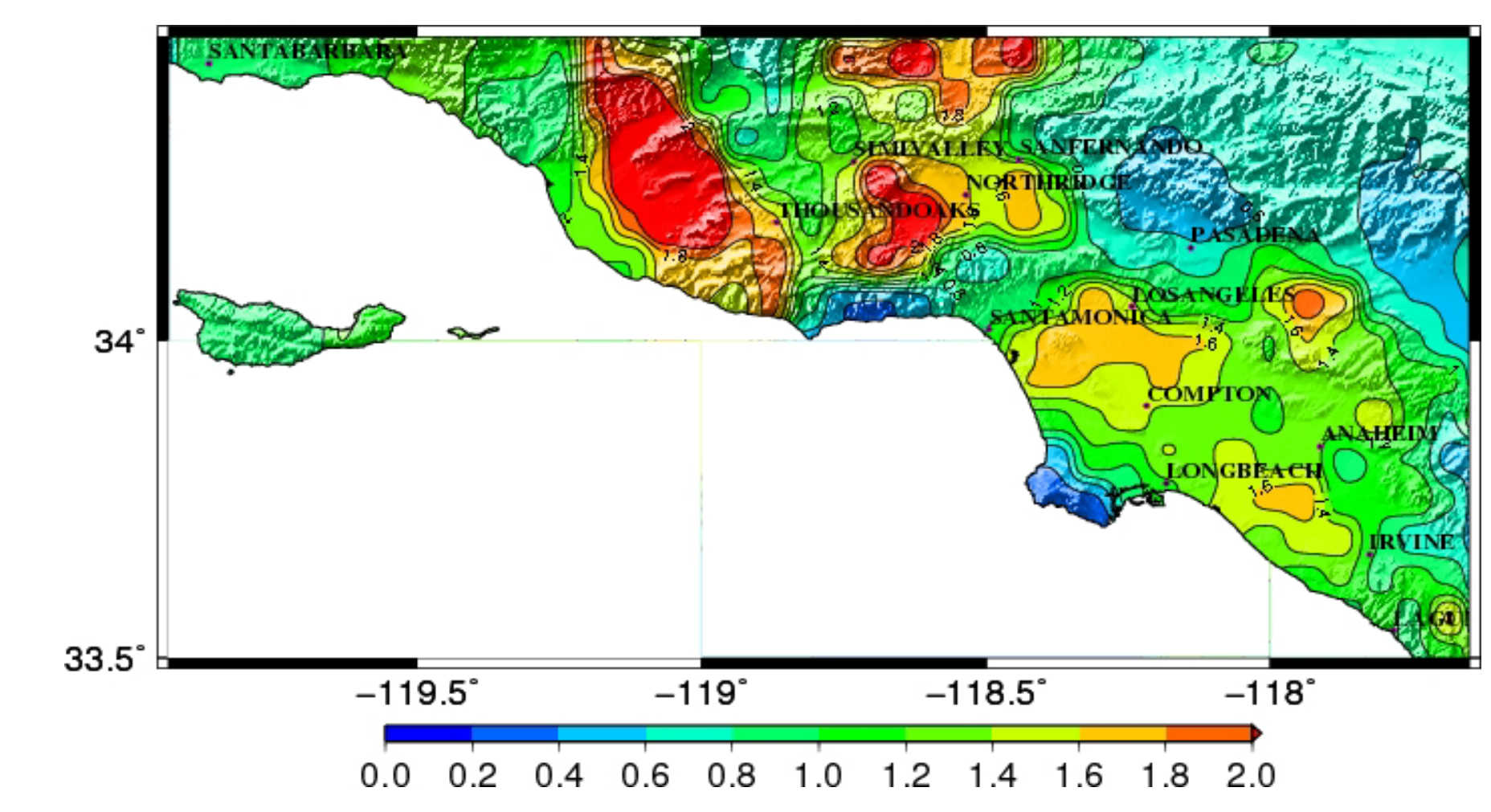
3-component ground motion wave forms are computed at 450 analysis sites spread across SoCal on a uniform grid of $7 \text{ km} \times 7 \text{ km}$ using SPEC3D.



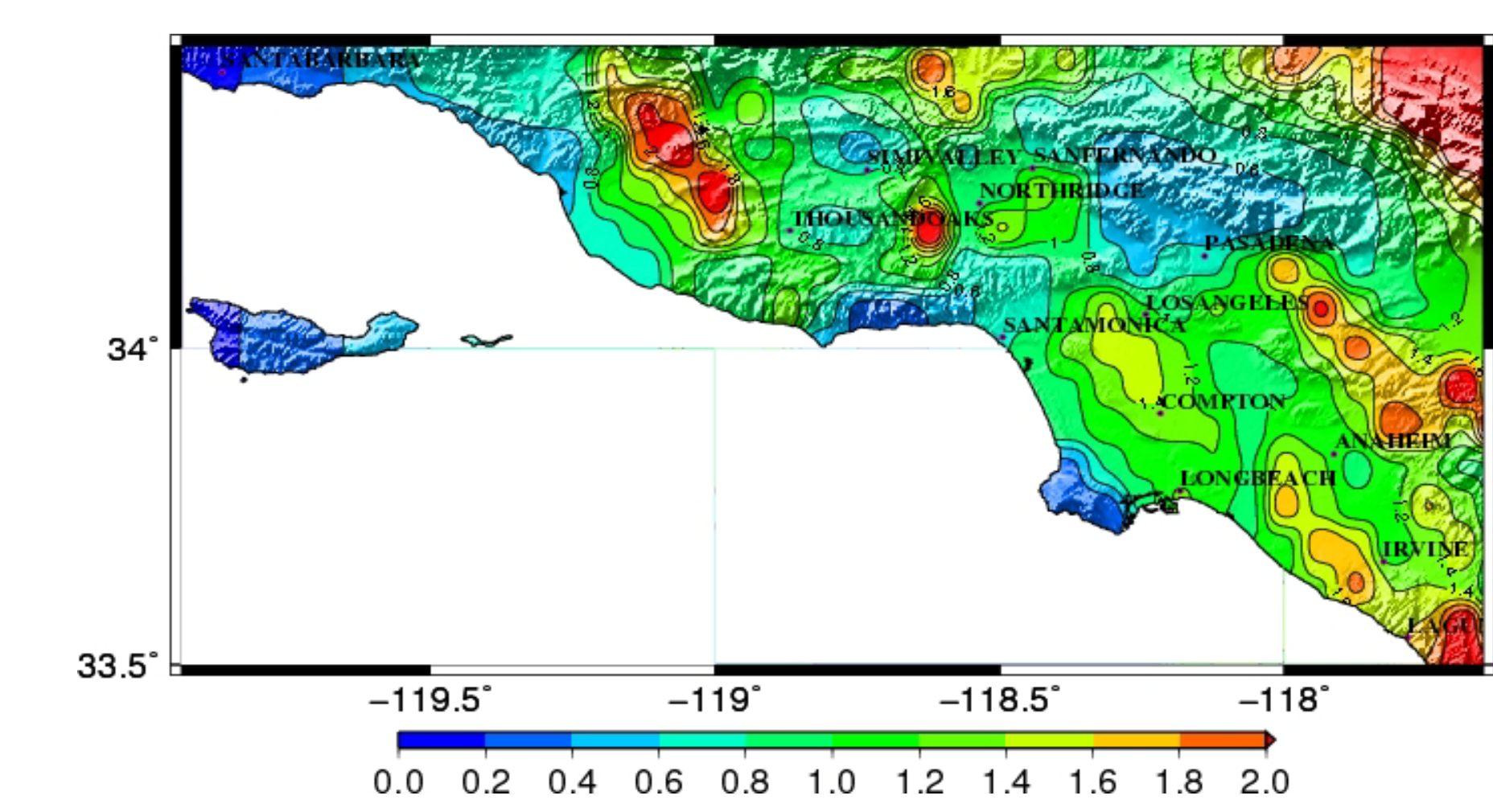
(c) Map of peak velocities (east component)



(d) Map of peak velocities (east component)



(e) Map of peak displacements (east component)



(f) Map of peak displacements (east component)

Fig.7: M_w 7.9 earthquake (north-to-south rupture) on San Andreas fault – ground shaking.

Note: Best-triangular fit source-time function to experimental data used for all sub faults in generating maps. Discrete source-time functions based on rupture velocity will be used for future ground shaking maps

6 Future Work

The ground motions generated will be used for conducting non-linear dynamic analysis of FRAME3D models for two steel moment frame buildings (20-story class) and one dual system building (40 story class) at each of the 450 sites across SoCal, the results of which will be used in probabilistic economic loss quantification.

7 References

- LU,X., LAPUSTA, N. & ROSAKIS,A.J. Pulse-like and crack-like ruptures in experiments mimicking crustal earthquakes. Proceedings of the National Academy of Sciences 104,48(2007),18931-18936.
SOMERVILLE,P.G.,IRIKURA,K.,GRAVES,R.,SAWADA,S.,WALD,D.,ABRAHAMSON,N.,IWASAKI,Y.,KAGAWA,T.,SMITH,N.,&KOWADA A. Characterizing crustal earthquake slip models for the prediction of strong ground motion. Seismological Research Letters 70,1(1999),59-80.
KLINGER,Y. Relation between continental strike-slip earthquake segmentation and thickness of the crust. Journal of Geophysical Research 115,B07306 (2010)

8 Acknowledgement

We gratefully acknowledge the funding provided by the National Science Foundation (NSF Award No. 0926962). We highly appreciate Dr. Rosakis (Caltech), Dr. Lapusta (Caltech) for making us avail their experimental data. We thank Dr. Heaton (Caltech), Dr. Ampuero (Caltech), Dr. Komatsch (Univ. of Pau, France), Dr. Mai (KAUST), Dr. Ji (UCSB), Dr. Bhat (Caltech) & others who have shared with their valuable insights of the project on various aspects. On a final note, we thank the Gordon and Betty Moore foundation for their support on this poster.